Engineering a Surfactant Trap via Post-Assembly Modification of an Imine Cage

María Pérez-Ferreiro,[a] Quinn M. Gallagher,[b] Andrea B. León,[a] Michael A. Webb,*[,b] Alejandro Criado,*[,a] and Jesús Mosquera*[,a]

[a]Universidade da Coruña, CICA−Centro Interdisciplinar de Química e Bioloxía, Rúa as Carballeiras, 15071 A Coruña, Spain
[b]Department of Chemical and Biological Engineering, Princeton University, Princeton, NJ 08544 USA

KEYWORDS: Imine cages, molecular self-assembly, host-guest chemistry, surfactants and post-assembly modifications.

ABSTRACT: Imine self-assembly stands as a potent strategy for preparing molecular organic cages. However, challenges persist, such as water insolubility and limited recognition properties due to constraints in the application of specific components during the self-assembly process. In this study, we addressed these limitations by initially employing a locking strategy, followed by a post-assembly modification. This sequential approach enables precise control over both the solubility and host-guest properties of an imine-based cage. The resulting structure demonstrates water solubility and exhibits an exceptional capacity to selectively interact with anionic surfactants, inducing their precipitation. Remarkably, each cage precipitates 24 equivalents of anionic surfactants even at concentrations much lower than the surfactant's critical micelle concentration (CMC), ensuring their complete removal. Molecular simulations elucidate how anionic surfactants specifically interact with the cage to facilitate aggregation below the surfactant CMC and induce precipitation as a micellar crosslinker. This innovative class of cages paves the way for the advancement of materials tailored for environmental remediation.

1. INTRODUCTION

The field of molecular cages is gaining substantial attention,[1–6] fueled by the tremendous potential they offer for biological applications,[7–10] catalysis,[11–13] and chemical separations.[14,15] Molecular self-assembly based on imine condensation has emerged as one the most effective approaches for synthesizing organic cages.[16–18] However, three major challenges have hindered their use: low solubility in aqueous media,[19,20] the imine bond instability in the presence of nucleophiles and water,[21,22] and the difficulties associated with using polar groups in the self-assembly process. Consequently, these cages have mainly been employed in the design of porous solid materials for gas separation and adsorption.[23,24]

The lability of imine bonds can be addressed by employing post-assembly covalent locking, converting imines to secondary amino groups.[25–27] However, addressing the challenge of poor water solubility proves more complex.[28,29] This issue arises from the need to incorporate rigid aromatic components into the self-assembly process to generate cavities, contributing to the hydrophobic nature of the resulting cages.[30,31] Additionally, the sensitivity of the imine self-assembly process to polar functionalities restricts the inclusion of polar groups in the cage, limiting both solubility and molecular recognition.

Surfactants, commonly referred to as "amphiphiles", are one the most applied supramolecular units in aqueous media for biological and industrial applications.[32,33] These molecules consist of a hydrophobic tail and a hydrophilic head. The hydrophobic part is usually formed of an aliphatic tail, whereas the polar head can vary according to its charge: non-ionic, cationic, anionic, or zwitterionic. The amphiphilic nature of these molecules enables them to self-assemble into supramolecular aggregates called micelles. As a result of their self-assembly properties in aqueous solution, surfactants have an extensive range of industrial applications. In fact, they are anticipated to exceed a global market value of $52 billion by 2025.[34]

Surfactants present a significant environmental risk, because of their impact on water animal and vegetal life. Additionally, some surfactants also have severe health implications on humans through ingestion or drinking of contaminated food items.[35] A promising avenue to remove surfactant is the use of synthetic host molecules that can selectively bind to surfactants. However, research in this area is limited, with only a few studies reporting that traditional hosts like cyclodextrins are capable of encapsulating a single molecule of surfactant without inducing precipitation.[39,40] Furthermore, the research team led by J.L. Sessler and X. Chi has recently utilized molecular cages to fabricate solid materials designed for the removal of fluorinated surfactants.[41,42]

Herein, we investigate the potential of a secondary post-assembly modification[43,44] of imine locked structures to enhance water solubility and induce novel recognition properties (Figure 1). Our research suggests that amide bond formation represents a suitable approach for attaching functionalities to the amino groups formed through post-assembly covalent locking. By implementing this approach, we achieved successful synthesis of a functionalized cage that exhibits solubility in both water and phosphate buffer. Furthermore, this cage displayed a

distinctive selectivity towards anionic surfactants, exhibiting a unique behavior by serving as a template agent for the formation of insoluble anionic micelles, resulting in the complete elimination of surfactants from the aqueous solution.

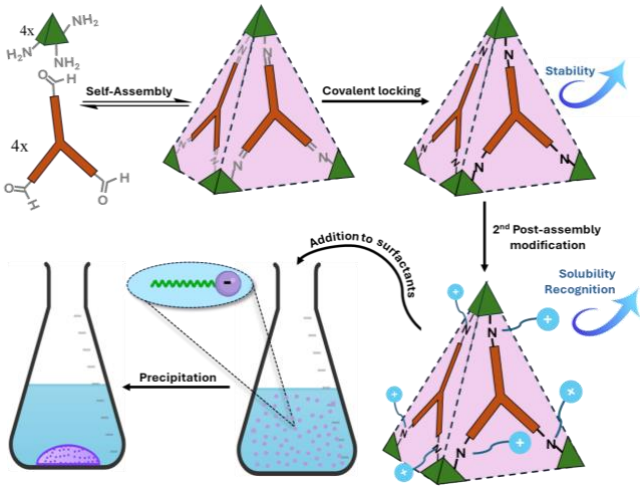

Figure 1. Schematic illustration of the synthetic approach to develop a molecular cage capable of precipitating anionic surfactants.

2. RESULTS AND DISCUSSION

Synthesis and characterization of A_4B_4 cage. Molecular cage **A_4B_4** was prepared using a one-pot Schiff base condensation involving 1,3,5-tris(aminomethyl)-2,4,6-trimethylbenzene (**A**) and tris(4-formylphenyl)amine (**B**). This process resulted in the formation of a tetrahedral imine-based cage with a cavity diameter of 10 Å, as previously reported by Cooper's group.[45] We found that this cage can undergo direct reduction in a one-pot reaction with the addition of sodium borohydride in methanol (Figure 2a). Nuclear magnetic resonance (NMR) and liquid chromatography-mass spectrometry (LC-MS) analyses unequivocally confirmed the successful formation of the covalent locked cage **A_4B_4** in quantitative yield (Fig. S3-8).

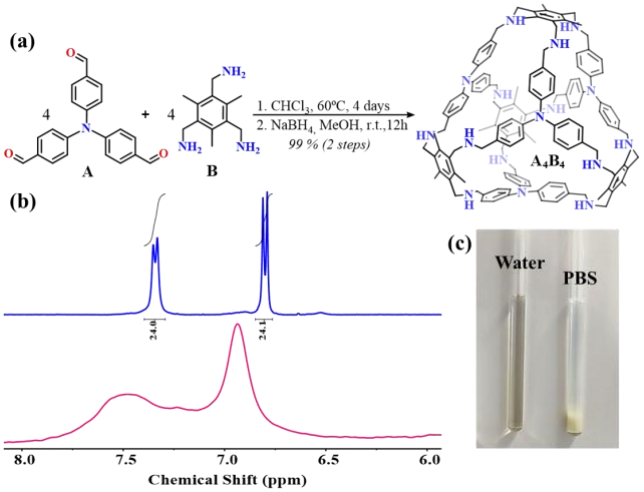

Figure 2. Synthesis and characterization of molecular cage **A_4B_4**. a) Preparation of the molecular cage. b) ^{1}H-NMR of **A_4B_4** in DMSO (blue) and D_2O (pink), showing one set of signals from the aromatic panel, where the broadening of the signals in water due to slow rotation can be observed. c) Comparison of the solubility of **A_4B_4** in both acidic water and PBS buffer.

The solubility of **A_4B_4** was assessed in both organic and aqueous solvents. When deprotonated, the cage is insoluble in common solvents and only partially soluble in dimethylformamide (DMF). However, upon protonation with either HCl or trifluoroacetic acid (TFA), **A_4B_4** displays substantially enhanced solubility in water, dimethyl sulfoxide (DMSO) and DMF. Consequently, ^{1}H-NMR spectroscopy could be utilized for further characterization of this compound. In deuterated DMSO, **A_4B_4** exhibits only one set of sharp ligand resonances (Figure 2b). This can be attributed to the rapid rotation of the aromatic rings within the cage, leading to a highly symmetric structure. Conversely, ^{1}H-NMR spectrum of the cage in acidic D_2O displays significantly broadened signals, suggesting a collapsed structure induced by hydrophobic effect (Figure 2b).

To determine the potential utility of **A_4B_4** in biological applications, its solubility was examined in phosphate-buffered saline (PBS) at neutral pH. Unfortunately, the cage was found to be insoluble in this medium (Figure 2c). This finding suggests that while the presence of secondary amino groups in organic cages enhances solubility in acidic conditions through protonation, this effect alone is insufficient to confer solubility at neutral pH. This may explain why the study of recognition properties of reduced organic cages has been limited to organic solvents.[46]

In addition to increased stability, covalent locking through imine reduction offers the advantage of forming secondary amino groups that can serve as valuable sites for binding additional functionalities through an extra post-assembly modification.[47] Until now, this strategy has exclusively demonstrated utility in the advancement of shape-persistent porous materials.[23,25] We opted to investigate the potential use of these amino groups to address the solubility constraints of **A_4B_4**. Specifically, we chose to attach positively charged pendants, aiming to not only impart water solubility but also enhance the cage's recognition abilities towards anionic molecules. Consequently, we synthesized a novel derivative, referred to as **p-A_4B_4** (Figure 3).

Synthesis and characterization of p-A_4B_4 cage. The synthesis of **p-A_4B_4** was accomplished through a straightforward method commonly employed in the synthesis of peptides.[48] The process involved incubating **A_4B_4** with an excess of the molecule 3-carboxy-N,N,N-trimethylpropan-1-aminium hexafluorophosphate, while utilizing the coupling agent hexafluorophosphate azabenzotriazole tetramethyl uronium (HATU). This resulted in the formation of an amide bond between the secondary amino groups of **A_4B_4** and the carboxylic group of the cationic molecule, ultimately yielding the desired product, **p-A_4B_4**. ^{1}H-NMR spectroscopy at room temperature displayed broad peaks in both water and DMSO, which were not useful for its characterization (Fig. S12-13). This was anticipated due to restricted rotation caused by the functionalization of the amino groups. ^{1}H-NMR spectrum in water at 90ºC lead to more defined signals, whose integrals agreed with the number of protons in **p-A_4B_4** (Fig. S14). To validate its identity and purity, conventional techniques used in biomolecule analysis, such as for peptides, were employed. High-resolution mass spectrometry was utilized for identification (Fig. 3). Reverse-phase HPLC was employed for both purification (preparative HPLC) and purity assessment (analytical HPLC) due to its ability to separate reaction intermediates in the formation of **p-A_4B_4** (Fig. S9).

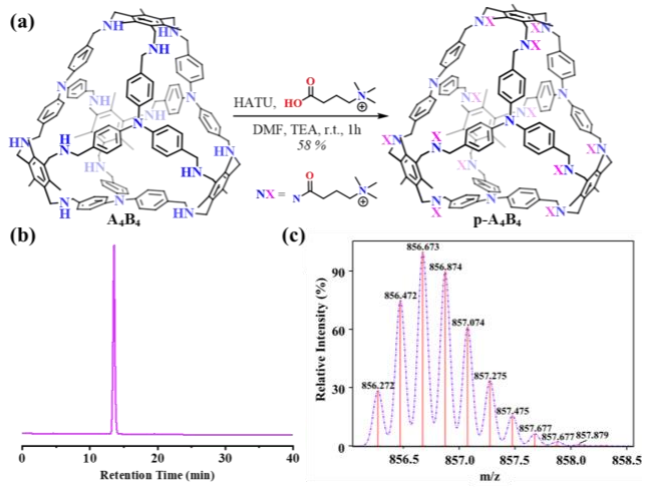

Figure 3. Synthesis and characterization of **p-A₄B₄.** a) Preparation of the molecular cage. b) HPLC chromatogram obtained for the purified **p-A₄B₄**. The conditions of the analysis went from 95% of water to 95% of acetonitrile, both with 0.1% of TFA, in 40 minutes. c) Predicted (purple profile) and obtained (red lines) MS spectra for **p-A₄B₄**. Spectrum shows *m/z* for $C_{216}H_{311}N_{28}O_{12}$ $[M+7TFA]^{5+}$.

In contrast to its precursor, **p-A₄B₄** showed a solubility of around 2.5 mg/mL in both water and PBS buffer at neutral pH. This characteristic prompted us to investigate its recognition abilities in aqueous environments. **p-A₄B₄** possesses a hydrophobic cavity surrounded by twelve positively charged pendants, making it a promising candidate for the recognition of hydrophobic anions. On this basis and the relevance of surfactants, we were motivated to investigate anionic surfactants as plausible guests.

Interaction between p-A₄B₄ and SDS surfactant. A fascinating outcome emerged when an aqueous solution of sodium dodecyl sulfate (SDS, 1 mM) was titrated with **p-A₄B₄**. As depicted in Figure 4, we observed the disappearance of the SDS signal and the concurrent formation of a solid within the NMR tube. What made this observation even more intriguing was the fact that a mere 0.04 equivalents of the cage sufficed to trigger the precipitation of all the SDS molecules. To quantify the reduction in the SDS signal, we conducted a titration using 1-ethyl-3-methylimidazolium chloride as an internal standard. Remarkably, it was observed that the reduction in SDS concentration exhibited a linear relationship with the addition of the cage with a slope of approximately -24 (Figure 4b). This finding suggests that each cage, possessing a charge of +12, has the capacity to induce the precipitation of 24 anionic SDS molecules. Essentially, this indicates the precipitation ability of two surfactant molecules per each positive charge within the cage. It's crucial to emphasize that the CMC of SDS is approximately 8 mM.[49] Therefore, SDS molecules are not forming micelles at the concentration employed in the titration.

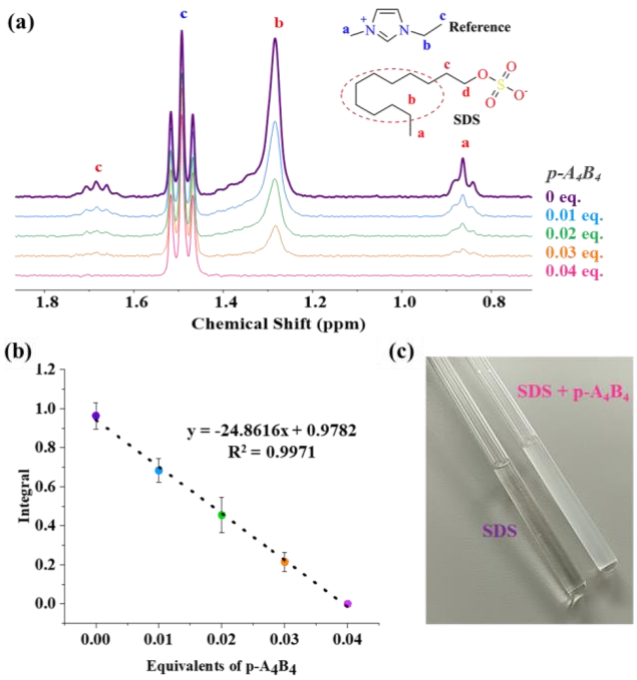

Figure 4. Interaction of **p-A₄B₄** with SDS. a) ^{1}H-NMR spectra for the titration of SDS (1 mM) with cage **p-A₄B₄** (from 0 to 0.04 equivalents) in D_2O, where the complete disappearance of the surfactant signal is observed. b) Linear fit for the titration, where the equivalents of **p-A₄B₄** are represented *vs* the surfactant's methyl group integral. c) Photo of the NMR tubes showing the precipitate formed after the addition of 0.04 equivalents of **p-A₄B₄** to the solution of SDS (1 mM).

To apply **p-A₄B₄** effectively for the removal of SDS molecules in practical applications, this cage must induce precipitation even in the presence of salts. To explore this, we prepared a solution containing SDS (1 mM) in a 10 mM PBS solution using deuterated water. Upon the addition of 0.04 equivalents of the cage, all the surfactant was removed, mirroring the outcome observed in pure water (Figure S24).

To assess the specificity of this phenomenon, we conducted similar experiments involving ^{1}H-NMR titrations in D_2O with hydrophobic anions distinct from surfactant molecules. Our selection comprised negatively charged aromatic compounds with varying numbers of sulfonate groups, which included tetra(4-sulfonatophenyl)porphyrin, 8-hydroxypyrene-1,3,6-trisulfonate, hexafluorophosphate and p-toluene sulfonate (Fig. S16-19). Remarkably, no precipitation of the guest molecules was observed, even when used in a one-to-one molar ratio.

Exploring the interaction of p-A₄B₄ with other surfactants. The previous observations with hydrophobic anions suggested that precipitation is not solely attributed to electrostatic interactions; rather, the aliphatic chain of SDS plays a significant role. To explore the relationship between the aliphatic chain and the precipitation phenomenon, we investigated two SDS analogues with aliphatic chains of varying lengths, both of which are negatively charged sulfonate surfactants. The initial analogue comprises a sulfonate headgroup in conjunction with a sixteen-carbon aliphatic chain, named **16C**, exhibiting a CMC of 0.22 mM.[50] In contrast, the second analog possesses a shorter tail comprising only six carbons, designated as **6C**. While this analog can serve as a cosurfactant, its abbreviated aliphatic tail restricts its ability to

independently self-assemble into micelles at concentrations lower than 1M.

When the **16C** surfactant is subjected to ^{1}H-NMR titration with **p-A$_4$B$_4$**, it exhibited behavior analogous to that of SDS, resulting in precipitation (Figure 5a). In this specific scenario, it was observed that to completely precipitate the surfactant, 0.05 equivalents of the cage were required, slightly exceeding the 0.04 equivalents needed for SDS. It is notable that the precipitation pattern exhibited by **p-A$_4$B$_4$** displayed a more pronounced sigmoidal shape compared to that observed with SDS (Figure 5d). These effects could stem from the surfactant's higher propensity to form micelles in comparison to SDS. Conversely, the **6C** exhibited behavior reminiscent of aromatic hydrophobic anions, as evidenced by ^{1}H-NMR spectroscopy, which revealed interactions but no precipitation (Figure 5b). During the titration with **p-A$_4$B$_4$**, a discernible trend was evident in the aliphatic signals of **6C** – they exhibited a consistent up-field shift and broadening, maintaining a constant integral.

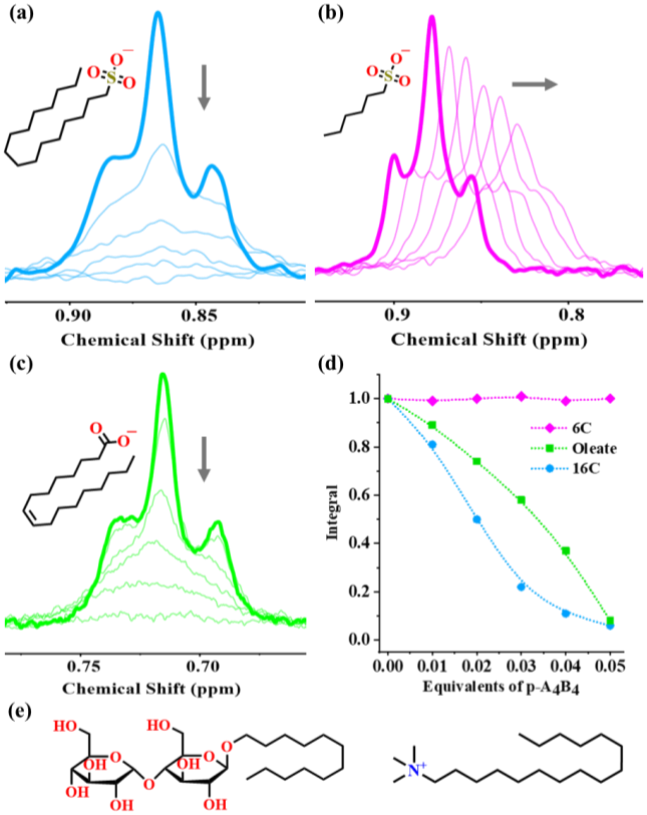

Figure 5. ^{1}H-NMR spectra (300 MHz, 298 K) for the titration of **p-A$_4$B$_4$** and three different surfactants (1 mM) with **p-A$_4$B$_4$** in D_2O. a) **16C**, b) **6C** and c) oleate. d) Representation of the data obtained from the titration of the former surfactants, showing the decrease in the signal corresponding to the terminal methyl group of each one. The represented data was the result of three different titrations for each surfactant. e) Structures of the surfactants that did not show interaction with **p-A$_4$B$_4$**: the neutral n-Dodecyl-β-D-maltoside (left) and the positively charged CTAB (right).

At this point, we decided to explore how general is the interaction of **p-A$_4$B$_4$** with surfactants. Consequently, we undertook an evaluation of this cage's interaction with sodium oleate. In contrast to previously examined surfactants, oleate features a carboxylate moiety as its polar headgroup, while its aliphatic tail comprises eighteen carbon atoms and a single unsaturation. Despite its distinct chemical structure compared to SDS, the outcomes closely resembled those observed with prior surfactants, demonstrating complete precipitation upon the addition of 0.05 equivalents of **p-A$_4$B$_4$** (Figure 5c). Subsequently, we shifted our focus to positively charged surfactants, particularly cetyltrimethylammonium bromide (CTAB), which has a 16-carbon aliphatic chain and a CMC of 1.0 mM.[33] Remarkably, **p-A$_4$B$_4$** did not exhibit any discernible interaction with CTAB by NMR (Fig. S30). Finally, we evaluated a neutral surfactant, n-Dodecyl-β-D-maltoside, featuring a 12-carbon aliphatic tail and a neutral polar head consisting of a disaccharide. However, as observed through ^{1}H-NMR titration, there was no interaction or precipitation, mirroring the results obtained with CTAB (Fig. S32).

These experiments underscore that the interaction of **p-A$_4$B$_4$** with other molecules is predominantly driven by electrostatic attraction, as it only exhibited interaction with anionic molecules. However, the precipitation phenomenon is specific to anionic surfactants. It is noteworthy that this precipitation occurs at concentrations significantly lower than the surfactant CMC.

Understanding cage-surfactant interaction. To gain a microscopic understanding of cage-surfactant interactions, we performed molecular dynamics (MD) simulations of **p-A$_4$B$_4$** in the presence of different surfactants in aqueous solution. We specifically examined interactions with SDS, CTAB and **6C** to evaluate effects related to ionic character and aliphatic tail length. Two scenarios were considered. In the first, systems featured a single **p-A$_4$B$_4$** in the presence of 48 surfactants to evaluate the nature of **p-A$_4$B$_4$**/surfactant interactions. In the second, systems featured three **p-A$_4$B$_4$** and surfactants to assess the propensity for precipitation via aggregation of multiple **p-A$_4$B$_4$**.

Figure 5a demonstrates that **p-A$_4$B$_4$** exhibits a significantly higher affinity for SDS compared to CTAB or **6C**. Initially, we conducted simulations with randomly distributed surfactants in a simulation cell, monitored their distances from **p-A$_4$B$_4$** over time, and employed clustering analysis to evaluate binding. These simulations showed that approximately 25-31 SDS molecules promptly bind to **p-A$_4$B$_4$**, while the number of bound CTAB and **6C** surfactants plateaus at lower values. The increased binding of **6C** compared to CTAB and the overall number of bound SDS aligns well with experimental findings. Because these simulations featured surfactant concentrations above the CMC, surfactants often formed small aggregates that would subsequently adsorb to **p-A$_4$B$_4$**, evident in the discrete jumps in Figure **6**a. To mimic interactions under more diluted conditions, additional simulations gradually introduced SDS to the cell, yet SDS continued to bind effectively to **p-A$_4$B$_4$** (SDS* in Figure **6**a). These findings suggest that the simulations accurately capture the essential physics of surfactant/**p-A$_4$B$_4$** systems, such as the relative affinity of **p-A$_4$B$_4$** towards anionic surfactants and the formation of aggregates under diluted conditions.

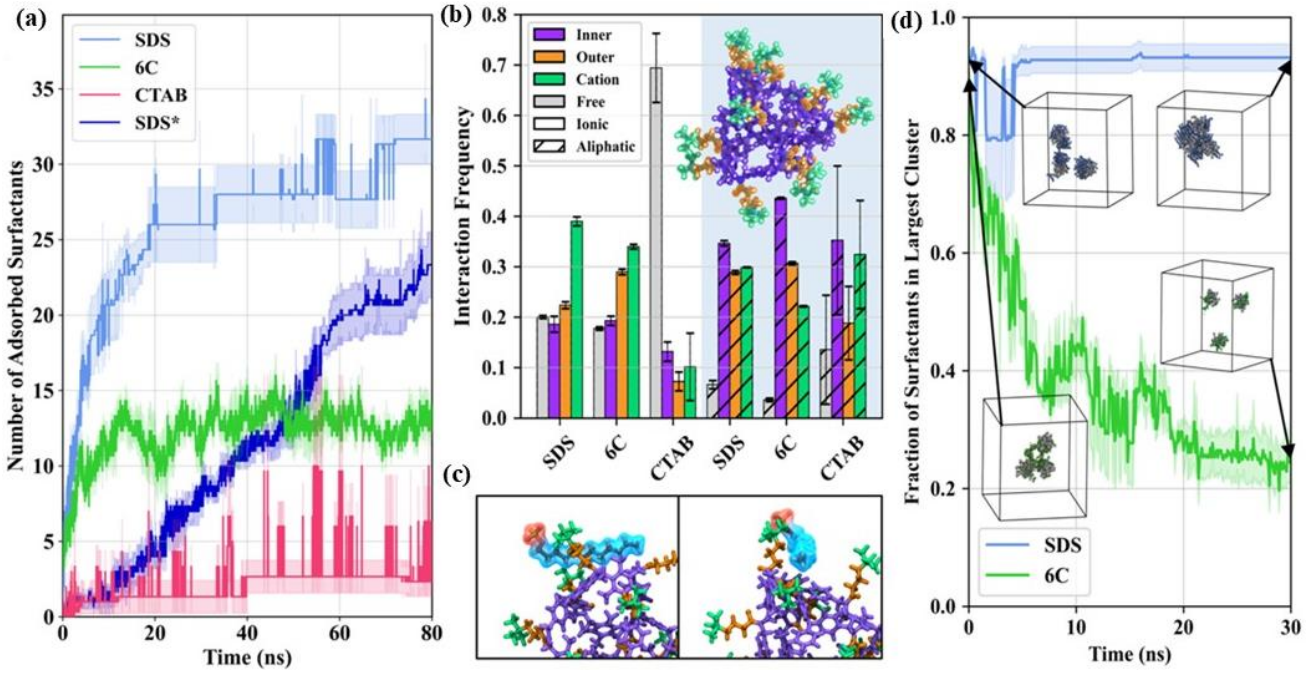

Figure 6. MD simulations of **p-A4B4** and surfactants. a) Number of surfactants in the vicinity of **p-A4B4** as a function of time. SDS* represents the gradual introduction of SDS into the cell to emulate dilution conditions. b) The relative frequency or proportion of charged (ionic, left) and neutral (aliphatic, right) groups of surfactant molecules interacting with inner, outer, or cationic regions of **p-A4B4**. Surfactant interactions with **p-A4B4** are defined if any atoms between the two groups are within 3.0 Å. Surfactants that are not in the vicinity of **p-A4B4** are labeled "free." The inset shows the decomposition of regions defined for **p-A4B4**, with the inner, outer, and cationic regions highlighted as purple, orange, and green, respectively. c) Representative simulation snapshot of SDS interacting with **p-A4B4**. The anionic head group is shown in red, while the aliphatic group is shown in blue. d) Fraction of surfactant molecules assigned to the largest aggregate for simulations with multiple **p-A4B4** units. Insets show **p-A4B4** molecules and their attached surfactants.

The enhanced binding of anionic surfactants led to a hypothesis that surfactants were specifically interacting with cationic portions of **p-A4B4**. To explore this, we monitored how often the ionic and aliphatic groups of adsorbed surfactants were interacting with the "inner" (derived from **A4B4**), "outer" (the neutral part of the pendants), and "cationic" (the positively charged quaternary ammonium) regions of **p-A4B4**. To characterize the relative proportion of such interactions, we define "interaction frequency" as the normalized number of occurrences where any atoms from the aliphatic or ionic portions of adsorbed surfactants **p-A4B4** were within a 3.0 Å radial cutoff of any atoms from a specified region of **p-A4B4**. Figure 6b reveals that the ionic group of anionic surfactants indeed preferentially interacts with cationic regions of **p-A4B4**. However, there are also a substantial number of interactions between aliphatic groups and all regions of **p-A4B4**. While behavior is relatively similar between SDS and **C6**, interactions between CTAB and **p-A4B4** are less specific, particularly for its ionic group. Across all surfactants, the aliphatic tails exhibit some preference towards the inner region of **p-A4B4**. Taken together, these results suggest that both electrostatic and dispersion interactions underlie the functionality of **p-A4B4**, as selective binding is principally driven by **p-A4B4**'s cationic functionalization, while the hydrophobic core region offers additional stabilizing interactions with aliphatic groups. In summary, these results elucidate why a single cage can precipitate 24 molecules of SDS. The interaction with surfactants takes place on the exterior of the cage, rather than through encapsulation within the cage cavity. As a result, the cage can accumulate a substantial number of surfactant molecules on its surface.

We next examined how the enhanced binding of anionic surfactants might manifest in observed precipitation. For this, single-**p-A4B4**/surfactant complexes from previous simulations involving SDS and **C6** were initialized in proximity and surrounded by additional surfactants to seed an aggregate of multiple **p-A4B4**; CTAB was not considered due to its prior minimal association with a single **p-A4B4**. Simulations were then run to assess whether such aggregates would remain stable. Figure 5d illustrates contrasting behavior between surfactants in terms of multi-cage assembly of **p-A4B4**. Although both SDS and **6C** both initially display large aggregates with multiple **p-A4B4** and most of the surfactants by virtue of the initialization procedure, such aggregates gradually dissipate for **6C** while they remain stable in the presence of SDS. Importantly, this observation facilitates comprehension regarding the exclusive ability of surfactants to enable multi-cage assembly. We hypothesize that this assembly process precedes subsequent precipitation events. I

3. CONCLUSIONS

We have achieved precise modulation of the solubility and host-guest properties in molecular cages, originating from imine self-assembly. This accomplishment is attributed to a dual-step post-assembly refinement: firstly, a covalent locking mechanism involving the reduction of imine bonds, and secondly, the harnessing of reactivity in the generated secondary amino groups to bind positively charged pendant groups. This modification not only rendered the cage water-soluble but also endowed it with a tailored affinity for anionic surfactant that enables their complete removal.

ASSOCIATED CONTENT

Supporting Information

The Supporting Information is available free of charge on the ACS Publications website.

Detailed experimental procedures, characterization (NMR spectroscopy, high-performance liquid chromatography [HPLC], HRMS spectrometry), and computational procedures are available in the supplemental information. Simulation files needed to reproduce the MD simulations are available at https://github.com/webbtheosim/surfactant-containers.

AUTHOR INFORMATION

Corresponding Authors

*mawebb@princeton.edu (M.A.W.); a.criado@udc.es (A.C.); j.mosquera1@udc.es (J.M.)

Further information and requests for resources should be directed to and will be fulfilled by the lead contact, J. Mosquera (j.mosquera1@udc.es).

Author Contributions

J.M. and A.C. conceived the project and designed the experiments. M.A.W. conceptualized simulations and theoretical calculations. M.P-F. and A.B.L. conducted the experimental part and Q.M.G performed the simulations and theoretical calculations. J.M., A.C., M.P-F, M.A.W., and Q.M.G. co-wrote the manuscript. All authors discussed and analyzed the results.

Notes

J.M, A.C. and M.P-F. are the inventors of a pending Spanish patent application.

ACKNOWLEDGMENT

This research was supported by the Xunta de Galicia under Project Proxectos de Excelencia (No. ED431F 2022/02). A. C. (RYC2020-030183-I and PID2021-127002NA-I00) and J. M. (RYC2019-027842-I and PID2020-117885GA-I00) acknowledge financial support by their grants funded by MCIN/AEI/10.13039/501100011033 and "ESF Investing in your future". M.A.W. acknowledges support from the National Science Foundation under Grant No. 2237470. Q.M.G acknowledges support by the National Science Foundation Graduate Research Fellowship Program under Grant No. DGE-2039656. Any opinions, findings, and conclusions or recommendations expressed in this material are those of the author(s) and do not necessarily reflect the views of the National Science Foundation.

REFERENCES

(1) McTernan, C. T.; Davies, J. A.; Nitschke, J. R. Beyond Platonic: How to Build Metal–Organic Polyhedra Capable of Binding Low-Symmetry, Information-Rich Molecular Cargoes. *Chem. Rev.* **2022**, *122* (11), 10393–10437. https://doi.org/10.1021/acs.chemrev.1c00763.

(2) Montà-González, G.; Sancenón, F.; Martínez-Máñez, R.; Martí-Centelles, V. Purely Covalent Molecular Cages and Containers for Guest Encapsulation. *Chem. Rev.* **2022**, *122* (16), 13636–13708. https://doi.org/10.1021/acs.chemrev.2c00198.

(3) Yang, X.; Ullah, Z.; Stoddart, J. F.; Yavuz, C. T. Porous Organic Cages. *Chem. Rev.* **2023**, *123* (8), 4602–4634. https://doi.org/10.1021/acs.chemrev.2c00667.

(4) Genov, G. R.; Takezawa, H.; Hayakawa, H.; Fujita, M. Tetradehydro-Diels–Alder Reactions of Flexible Arylalkynes via Folding Inside a Molecular Cage. *J. Am. Chem. Soc.* **2023**, *145* (31), 17013–17017. https://doi.org/10.1021/jacs.3c06301.

(5) Percástegui, E. G.; Ronson, T. K.; Nitschke, J. R. Design and Applications of Water-Soluble Coordination Cages. *Chem. Rev.* **2020**, *120* (24), 13480–13544. https://doi.org/10.1021/acs.chemrev.0c00672.

(6) Lewis, J. E. M. Developing Sophisticated Microenvironments in Metal-Organic Cages. *Trends Chem.* **2023**, *5* (10), 717–719. https://doi.org/10.1016/j.trechm.2023.06.003.

(7) Küng, R.; Pausch, T.; Rasch, D.; Göstl, R.; Schmidt, B. M. Mechanochemical Release of Non-Covalently Bound Guests from a Polymer-Decorated Supramolecular Cage. *Angew. Chem. Int. Ed.* **2021**, *60* (24), 13626–13630. https://doi.org/10.1002/anie.202102383.

(8) Fernández-Caro, H.; Lostalé-Seijo, I.; Martínez-Calvo, M.; Mosquera, J.; L. Mascareñas, J.; Montenegro, J. Supramolecular Caging for Cytosolic Delivery of Anionic Probes. *Chem. Sci.* **2019**, *10* (39), 8930–8938. https://doi.org/10.1039/C9SC02906K.

(9) Ghosh, C.; Ali, L. M. A.; Bessin, Y.; Clément, S.; Richeter, S.; Bettache, N.; Ulrich, S. Self-Assembled Porphyrin–Peptide Cages for Photodynamic Therapy. *Org. Biomol. Chem.* **2024**, *22* (7), 1484–1494. https://doi.org/10.1039/D3OB01887C.

(10) Montà-González, G.; Ortiz-Gómez, E.; López-Lima, R.; Fiorini, G.; Martínez-Máñez, R.; Martí-Centelles, V. Water-Soluble Molecular Cages for Biological Applications. *Molecules* **2024**, *29* (7), 1621. https://doi.org/10.3390/molecules29071621.

(11) Piskorz, T. K.; Martí-Centelles, V.; Spicer, R. L.; Duarte, F.; Lusby, P. J. Picking the Lock of Coordination Cage Catalysis. *Chem. Sci.* **2023**, *14* (41), 11300–11331. https://doi.org/10.1039/D3SC02586A.

(12) Ham, R.; Nielsen, C. J.; Pullen, S.; Reek, J. N. H. Supramolecular Coordination Cages for Artificial Photosynthesis and Synthetic Photocatalysis. *Chem. Rev.* **2023**, *123* (9), 5225–5261. https://doi.org/10.1021/acs.chemrev.2c00759.

(13) Li, X.; Lin, W.; Sharma, V.; Gorecki, R.; Ghosh, M.; Moosa, B. A.; Aristizabal, S.; Hong, S.; Khashab, N. M.; Nunes, S. P. Polycage Membranes for Precise Molecular Separation and Catalysis. *Nat. Commun.* **2023**, *14* (1), 3112. https://doi.org/10.1038/s41467-023-38728-7.

(14) Ghosh, A.; Pruchyathamkorn, J.; Fuertes Espinosa, C.; Nitschke, J. R. Light-Driven Purification of Progesterone from Steroid Mixtures Using a Photoresponsive Metal–Organic Capsule. *J. Am. Chem. Soc.* **2024**, *146* (4), 2568−2573. https://doi.org/10.1021/jacs.3c11005.

(15) Zhang, D.; Ronson, T. K.; Zou, Y.-Q.; Nitschke, J. R. Metal–Organic Cages for Molecular Separations. *Nat. Rev. Chem.* **2021**, *5* (3), 168–182. https://doi.org/10.1038/s41570-020-00246-1.

(16) Acharyya, K.; Mukherjee, P. S. Organic Imine Cages: Molecular Marriage and Applications. *Angew. Chem. Int. Ed.* **2019**, *58* (26), 8640–8653. https://doi.org/10.1002/anie.201900163.

(17) Yang, Z.; Esteve, F.; Antheaume, C.; Lehn, J.-M. Dynamic Covalent Self-Assembly and Self-Sorting Processes in the Formation of Imine-Based Macrocycles and Macrobicyclic Cages. *Chem. Sci.* **2023**, *14* (24), 6631–6642. https://doi.org/10.1039/D3SC01174G.

(18) Lu, Y.-L.; Zhang, X.-D.; Qin, Y.-H.; Song, J.-Q.; Huang, Y.-H.; Liu, C.-H.; Chen, J.-J.; Xu, H.-S.; Pan, M.; Su, C.-Y. A Robust Protein-Mimicking Metallo-Amine Cage Showing Proton-Driven Allostery with Water as the Effector. *Chem* **2023**, *9* (8), 2144–2160. https://doi.org/10.1016/j.chempr.2023.03.019.

(19) Koo, J.; Kim, I.; Kim, Y.; Cho, D.; Hwang, I.-C.; Mukhopadhyay, R. D.; Song, H.; Ko, Y. H.; Dhamija, A.; Lee, H.; Hwang, W.; Kim, S.; Baik, M.-H.; Kim, K. Gigantic Porphyrinic Cages. *Chem* **2020**, *6* (12), 3374–3384. https://doi.org/10.1016/j.chempr.2020.10.002.

(20) Wagner, P.; Rominger, F.; Zhang, W.-S.; Gross, J. H.; Elbert, S. M.; Schröder, R. R.; Mastalerz, M. Chiral Self-Sorting of Giant Cubic [8+12] Salicylimine Cage Compounds. *Angew. Chem. Int. Ed.* **2021**, *60* (16), 8896–8904. https://doi.org/10.1002/anie.202016592.

(21) Lei, Y.; Chen, Q.; Liu, P.; Wang, L.; Wang, H.; Li, B.; Lu, X.; Chen, Z.; Pan, Y.; Huang, F.; Li, H. Molecular Cages Self-Assembled by Imine Condensation in Water. *Angew. Chem. Int. Ed.* **2021**, *60* (9), 4705–4711. https://doi.org/10.1002/anie.202013045.

(22) Chen, Y.; Tang, H.; Chen, H.; Li, H. Self-Assembly via Condensation of Imine or Its N-Substituted Derivatives. *Acc. Chem. Res.* **2023**, *56* (20), 2838–2850. https://doi.org/10.1021/acs.accounts.3c00475.

(23) Liu, M.; Zhang, L.; Little, M. A.; Kapil, V.; Ceriotti, M.; Yang, S.; Ding, L.; Holden, D. L.; Balderas-Xicohténcatl, R.; He, D.; Clowes, R.; Chong, S. Y.; Schütz, G.; Chen, L.; Hirscher, M.; Cooper, A. I. Barely Porous Organic Cages for Hydrogen Isotope Separation. *Science* **2019**, *366* (6465), 613–620. https://doi.org/10.1126/science.aax7427.

(24) He, A.; Jiang, Z.; Wu, Y.; Hussain, H.; Rawle, J.; Briggs, M. E.; Little, M. A.; Livingston, A. G.; Cooper, A. I. A Smart and Responsive Crystalline Porous Organic Cage Membrane with Switchable Pore Apertures for Graded Molecular Sieving. *Nat. Mater.* **2022**, *21* (4), 463–470. https://doi.org/10.1038/s41563-021-01168-z.

(25) Mastalerz, M. Porous Shape-Persistent Organic Cage Compounds of Different Size, Geometry, and Function. *Acc. Chem. Res.* **2018**, *51* (10), 2411–2422. https://doi.org/10.1021/acs.accounts.8b00298.

(26) Lin, W.; Zhang, G.; Zhu, X.; Yu, P.; Alimi, L. O.; Moosa, B. A.; Sessler, J. L.; Khashab, N. M. Caging the Hofmeister Effect by a Biomimetic Supramolecular Receptor. *J. Am. Chem. Soc.* **2023**, *145* (23), 12609–12616. https://doi.org/10.1021/jacs.3c01849.

(27) Qin, Y.; Ling, Q.-H.; Wang, Y.-T.; Hu, Y.-X.; Hu, L.; Zhao, X.; Wang, D.; Yang, H.-B.; Xu, L.; Tang, B. Z. Construction of Covalent Organic Cages with Aggregation-Induced Emission Characteristics from Metallacages for Mimicking Light-Harvesting Antenna. *Angew. Chem. Int. Ed.* **2023**, *62* (36), e202308210. https://doi.org/10.1002/anie.202308210.

(28) Chakraborty, D.; Mukherjee, P. S. Recent Trends in Organic Cage Synthesis: Push towards Water-Soluble Organic Cages. *Chem. Commun.* **2022**, *58* (37), 5558–5573. https://doi.org/10.1039/D2CC01014C.

(29) Chen, Q.; Li, Z.; Lei, Y.; Chen, Y.; Tang, H.; Wu, G.; Sun, B.; Wei, Y.; Jiao, T.; Zhang, S.; Huang, F.; Wang, L.; Li, H. The Sharp Structural Switch of Covalent Cages Mediated by Subtle Variation of Directing Groups. *Nat. Commun.* **2023**, *14* (1), 4627. https://doi.org/10.1038/s41467-023-40255-4.

(30) Hong, S.; Rohman, Md. R.; Jia, J.; Kim, Y.; Moon, D.; Kim, Y.; Ko, Y. H.; Lee, E.; Kim, K. Porphyrin Boxes: Rationally Designed Porous Organic Cages. *Angew. Chem. Int. Ed.* **2015**, *54* (45), 13241–13244. https://doi.org/10.1002/anie.201505531.

(31) Benke, B. P.; Kirschbaum, T.; Graf, J.; Gross, J. H.; Mastalerz, M. Dimeric and Trimeric Catenation of Giant Chiral [8 + 12] Imine Cubes Driven by Weak Supramolecular Interactions. *Nat. Chem.* **2023**, *15* (3), 413–423. https://doi.org/10.1038/s41557-022-01094-w.

(32) González-Rubio, G.; Mosquera, J.; Kumar, V.; Pedrazo-Tardajos, A.; Llombart, P.; Solís, D. M.; Lobato, I.; Noya, E. G.; Guerrero-Martínez, A.; Taboada, J. M.; Obelleiro, F.; MacDowell, L. G.; Bals, S.; Liz-Marzán, L. M. Micelle-Directed Chiral Seeded Growth on Anisotropic Gold Nanocrystals. *Science* **2020**, *368* (6498), 1472–1477. https://doi.org/10.1126/science.aba0980.

(33) Su, L.; Mosquera, J.; Mabesoone, M. F. J.; Schoenmakers, S. M. C.; Muller, C.; Vleugels, M. E. J.; Dhiman, S.; Wijker, S.; Palmans, A. R. A.; Meijer, E. W. Dilution-Induced Gel-Sol-Gel-Sol Transitions by Competitive Supramolecular Pathways in Water. *Science* **2022**, *377* (6602), 213–218. https://doi.org/10.1126/science.abn3438.

(34) Badmus, S. O.; Amusa, H. K.; Oyehan, T. A.; Saleh, T. A. Environmental Risks and Toxicity of Surfactants: Overview of Analysis, Assessment, and Remediation Techniques. *Environ. Sci. Pollut. Res.* **2021**, *28* (44), 62085–62104. https://doi.org/10.1007/s11356-021-16483-w.

(35) Badmus, S. O.; Amusa, H. K.; Oyehan, T. A.; Saleh, T. A. Environmental Risks and Toxicity of Surfactants: Overview of Analysis, Assessment, and Remediation Techniques. *Environ. Sci. Pollut. Res.* **2021**, *28* (44), 62085–62104. https://doi.org/10.1007/s11356-021-16483-w.

(36) Basar, C. A.; Karagunduz, A.; Cakici, A.; Keskinler, B. Removal of Surfactants by Powdered Activated Carbon and Microfiltration. *Water Res.* **2004**, *38* (8), 2117–2124. https://doi.org/10.1016/j.watres.2004.02.001.

(37) Louhichi, B.; Ahmadi, M. F.; Bensalah, N.; Gadri, A.; Rodrigo, M. A. Electrochemical Degradation of an Anionic Surfactant on Boron-Doped Diamond Anodes. *J. Hazard. Mater.* **2008**, *158* (2), 430–437. https://doi.org/10.1016/j.jhazmat.2008.01.093.

(38) Siyal, A. A.; Shamsuddin, M. R.; Low, A.; Rabat, N. E. A Review on Recent Developments in the Adsorption of Surfactants from Wastewater. *J. Environ. Manage.* **2020**, *254*, 109797. https://doi.org/10.1016/j.jenvman.2019.109797.

(39) dos Santos Silva Araújo, L.; Lazzara, G.; Chiappisi, L. Cyclodextrin/Surfactant Inclusion Complexes: An Integrated View of Their Thermodynamic and Structural Properties. *Adv. Colloid Interface Sci.* **2021**, *289*, 102375. https://doi.org/10.1016/j.cis.2021.102375.

(40) Hao, L.-S.; Wang, H.-X.; Wang, Y.-S.; Meng, Y.-Q.; Nan, Y.-Q. Inclusion Complexation of Surfactant with β-Cyclodextrin and Its Effect on the Mixed Micellization of Cationic/Anionic Surfactants. *Colloids Surf. Physicochem. Eng. Asp.* **2023**, *668*, 131437. https://doi.org/10.1016/j.colsurfa.2023.131437.

(41) He, Y.; Zhou, J.; Li, Y.; Yang, Y.-D.; Sessler, J. L.; Chi, X. Fluorinated Nonporous Adaptive Cages for the Efficient Removal of Perfluorooctanoic Acid from Aqueous Source Phases. *J. Am. Chem. Soc.* **2024**, *146* (9), 6225–6230. https://doi.org/10.1021/jacs.3c14213.

(42) He, Y.; Luo, D.; Lynch, V. M.; Ahmed, M.; Sessler, J. L.; Chi, X. Porous Adaptive Luminescent Metallacage for the Detection and Removal of Perfluoroalkyl Carboxylic Acids. *Chem* **2023**, *9* (1), 93–101. https://doi.org/10.1016/j.chempr.2022.09.004.

(43) Wang, H.; Jin, Y.; Sun, N.; Zhang, W.; Jiang, J. Post-Synthetic Modification of Porous Organic Cages. *Chem. Soc. Rev.* **2021**, *50* (16), 8874–8886. https://doi.org/10.1039/D0CS01142H.

(44) Roberts, D. A.; Pilgrim, B. S.; Nitschke, J. R. Covalent Post-Assembly Modification in Metallosupramolecular Chemistry. *Chem. Soc. Rev.* **2018**, *47* (2), 626–644. https://doi.org/10.1039/C6CS00907G.

(45) Greenaway, R. L.; Santolini, V.; Bennison, M. J.; Alston, B. M.; Pugh, C. J.; Little, M. A.; Miklitz, M.; Eden-Rump, E. G. B.; Clowes, R.; Shakil, A.; Cuthbertson, H. J.; Armstrong, H.; Briggs, M. E.; Jelfs, K. E.; Cooper, A. I. High-Throughput Discovery of Organic Cages and Catenanes Using Computational Screening Fused with Robotic Synthesis. *Nat. Commun.* **2018**, *9* (1), 2849. https://doi.org/10.1038/s41467-018-05271-9.

(46) Acharyya, K.; Mukherjee, P. S. A Fluorescent Organic Cage for Picric Acid Detection. *Chem. Commun.* **2014**, *50* (99), 15788–15791. https://doi.org/10.1039/C4CC06225F.

(47) Acharyya, K.; Mukherjee, P. S. Postsynthetic Exterior Decoration of an Organic Cage by Copper(I)-Catalysed A3-Coupling and Detection of Nitroaromatics. *Chem. – Eur. J.* **2015**, *21* (18), 6823–6831. https://doi.org/10.1002/chem.201406581.

(48) McKnelly, K. J.; Sokol, W.; Nowick, J. S. Anaphylaxis Induced by Peptide Coupling Agents: Lessons Learned from Repeated Exposure to HATU, HBTU, and HCTU. *J. Org. Chem.* **2020**, *85* (3), 1764–1768. https://doi.org/10.1021/acs.joc.9b03280.

(49) Stanley, F. E.; Warner, A. M.; Schneiderman, E.; Stalcup, A. M. Rapid Determination of Surfactant Critical Micelle Concentrations Using Pressure-Driven Flow with Capillary Electrophoresis Instrumentation. *J. Chromatogr. A* **2009**, *1216* (47), 8431–8434. https://doi.org/10.1016/j.chroma.2009.09.026.

(50) Kumar, H.; Kaur, G. Deciphering Aggregation Behavior and Thermodynamic Properties of Anionic Surfactant Sodium Hexadecyl Sulfate in Aqueous Solutions of Ionic Liquids [C5mim][Br] and [C6mim][Br]. *J. Mol. Liq.* **2020**, *298*, 111949. https://doi.org/10.1016/j.molliq.2019.111949.

(51) Annunziata, O.; Costantino, L.; D'Errico, G.; Paduano, L.; Vitagliano, V. Transport Properties for Aqueous Sodium Sulfonate Surfactants: 2. Intradiffusion Measurements: Influence of the Obstruction Effect on the Monomer and Micelle Mobilities. *J. Colloid Interface Sci.* **1999**, *216* (1), 16–24. https://doi.org/10.1006/jcis.1999.6269.

Table of Contents artwork